Proceedings of the
Annual Stability Conference
Structural Stability Research Council
Atlanta, Georgia, April 21-24, 2020

Local buckling analysis of multi-sided steel tube sections

Zannatul Mawa Dalia[1], Anjan Bhowmick[2]

Abstract
Multi-sided steel tubular sections are commonly used in many structures such as light posts, road signpost, transmission and telecommunication towers, etc. These sections are generally subjected to axial compression, pure bending, combined bending and compression or torsion. From the design point of view, it is essential to make sure that these thin-walled sections do not buckle locally before reaching their capacities. Unlike Canadian bridge design standard (CSA S6-14), current AASHTO standard for structural supports for highway signs, luminaires, and traffic signals provides slenderness limits to check for local buckling of Octagonal (8-sides), Dodecagonal (12-sides) and Hexadecagonal (16-sides) steel tube sections when they are subjected to axial compression and bending. Although many structures now use these multi-sided sections, very limited study has been conducted to evaluate slenderness limits of these thin-walled sections. This paper presents a finite element (FE) analysis based study of local buckling of multi-sided steel tubular sections. A nonlinear finite element model is developed for this study. The finite element model is validated against experimental results from stub column tests of 8, 12, and 16-sided cross-sections. The validated FE model is then used to analyze a series of multi-sided steel tubular sections subjected to axial compression, pure bending, and torsion. Results from FE analyses are used to evaluate the slenderness limits specified in different standards (AASHTO, ASCE, and Eurocode). FE analyses show that the compact limit in the AASHTO standard might need to be revised, whereas the non-compact limit is more relaxing for sections under pure bending. Moreover, FE analyses also indicate that the non-compact limit of the Hexadecagonal section can be used for the other two sections under axial compression.

1. Introduction

Multi-sided tube sections are hollow sections having a polygonal cross-section. These thin-walled sections are used in many structures like overhead road signpost, light post, transmission pole, etc. These structures are generally subjected to axial compression, pure bending, combined bending and compression or torsion. These thin-walled sections tend to buckle locally if proper width-thickness ratios are not maintained. Local buckling of multi-sided tube section must be prevented until the member can reach its capacity. This will ensure the adequate service life of the structure.

[1] Graduate Research Assistant, Concordia University, <zannatdaliace09@gmail.com>
[2] Associate Professor, Concordia University, <anjan.bhowmick@concordia.ca>

Elastic buckling stress of a single plate can be obtained by using Timoshenko's equation (Timoshenko, 1961). Multi-sided tubular sections can be considered as an assembly of restrained plates to determine the elastic critical buckling stress using the familiar equation of Timoshenko, as shown in Eq. 1:

$$\sigma_{cr} = \frac{k\pi^2 E}{12(1-\nu^2)\left(\frac{b}{t}\right)^2} \quad (1)$$

where *k* is the plate buckling coefficient determined by theoretical critical-load analysis and is a function of plate geometry and boundary conditions; *E*, *v*, *b* and *t* are the modulus of elasticity, poison's ratio, plate width, and plate thickness, respectively. For simply supported plate, a *k* value of 4.0 can be used. Several studies have been undertaken to find values of *k* for different geometry, loading, and support conditions.

There have been some studies on behavior of multi-sided steel tube sections under different loading conditions. Wittrick et al. (1968) developed a "Stability Function" based theoretical method to develop criteria for local buckling analyses of polygonal tubular sections subjected to combined compression and torsion and reported the critical combination of compression and torsion for three and four-sided polygonal tube sections. Aoki et al. (1991) experimentally investigated the local buckling behavior of polygonal steel sections of four to eight sides under compression. They have observed that strength of specimen is closely related to plate width-thickness parameter (*R*), as defined by Eq. 2:

$$R = \sqrt{\frac{F_y}{\sigma_{cr}}} \quad (2)$$

where F_y is the yield stress, and σ_{cr} can be obtained from Eq.1.

Teng et al. (1999) studied the elastic local buckling behavior of columns having polygonal cross-sections (4- to 8- sided) under uniform axial compression or bending by using the finite strip method and reported plate buckling coefficients (*k*-values) for different slenderness ratios. Godat et al. (2012) conducted an experimental study to investigate elastoplastic local buckling behavior of thin-walled tubes having polygonal cross-sections (i.e., 8-, 12-, and 16-sided) under concentric compression. Critical local buckling stress has been observed for different plate width-thickness ratios. Gonçalves et al. (2013) investigated the elastic buckling behavior of the tubular section having regular polygonal cross-section under uniform compression by using specialized Generalized Beam Theory (GBT). For pure local buckling, it was found that minimum critical buckling stress of even-sided sections can be predicted by using a buckling coefficient (*k*) of 4.0. For the odd-sided sections (i.e., 3-, 5-, and 7- sided), *k*-values were reported to be higher than 4.0. Bräutigam et al. (2017) experimentally and numerically investigated the bending behavior of sixteen (16) sided polygonal tubular steel sections under pure bending and combined bending and torsion. Their study indicated that bending moment capacity for compact section can be more than the elastic bending moment capacity (yield moment). It was also reported that it might not be appropriate to use the full plastic moment capacity (M_p) of 16-sided polygonal tubular section.

Current AASHTO (2015) provides nominal strengths of multi-sided tubular sections subjected to compression, tension, bending, shear, and combined forces. ASCE (ASCE/SEI-48-11, 2011) provides design equations for local buckling capacities of eight, twelve, and sixteen-sided polygonal steel sections of the transmission line. Eurocode 3 (EN 1-1, 2005, EN 1-3, 2006, EN 1-5, 2006) has design equation for plate elements. In this study, a multi-sided steel tubular section has been considered as a collection of individual longitudinal plate strips to find the resistance using Eurocode 3. AASHTO also provides width-thickness limits for eight, twelve, and sixteen-sided polygonal steel sections. While AASHTO recommends same width-thickness limit for all the three sections when they are compact, the requirements are different for non-compact sections. However, very limited study has been conducted to evaluate these limits. The objective of this study is to observe the local buckling behavior of the multi-sided steel tubular section subjected to axial compression, pure bending, and torsion by developing Finite Element Models (FEM). FE analysis results have been compared with the existing codes. Three different types of geometry, eight (8), twelve (12), and sixteen (16) sided polygonal sections, are considered.

2. Finite Element Modeling

A nonlinear finite element model is developed using ABAQUS software. Both material and geometric nonlinearities have been incorporated in the model. The following subsections describe the details of FE model development.

2.1 Elements and Properties

Thin-walled members having three different polygonal cross-sections (i.e., Octagonal, Dodecagonal, and Hexadecagonal), as shown in Fig. 1, have been modeled using 4-node shell elements with reduced integration (S4R from ABAQUS element library) (ABAQUS, 2014). Moreover, mesh sensitivity analysis has been conducted to get a suitable mesh size for each polygonal cross-section.

2.2 Boundary Conditions

A simply supported boundary condition was adopted for analyses of multi-sided tube sections subjected to bending and pure compression. For the simply supported boundary condition:

i. Right end was restrained against X, Y and Z-axis deflection (U1= U2= U3= 0) and rotation about Z-axis (UR3=0). Rotation about X and Y-axis was kept unrestrained.
ii. The left end was restrained against X and Y-axis deflection (U1= U2= 0) and rotation about Z-axis (UR3=0). Rotation about X and Y-axis and deflection in Z-axis were kept unrestrained.

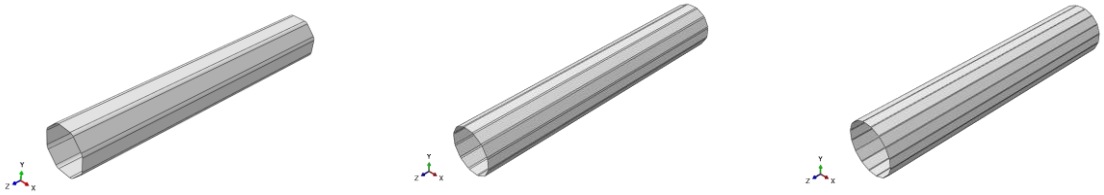

(a) Octagonal section (b) Dodecagonal section (c) Hexadecagonal section

Figure 1: Selected steel multi-sided tube sections

For pure torsional loading, one end of the member had fixed boundary condition and the remaining end was free. At the fixed end, deflection in X, Y, and Z-axis (U1= U2= U3= 0) and rotation about X, Y, and Z-axis (UR1=UR2=UR3=0) were restrained. However, at the free end, deflection in X and Y-axis (U1= U2= 0) were kept restrained.

2.3 Material properties

Bilinear elastoplastic stress versus strain curve has been used for all the models. A strain-hardening of 2% of modulus of elasticity (E) of steel has been used. Modulus of elasticity (E) of 200 GPa, Yield stress (F_y) of 345 MPa, and poison's (v) ratio of 0.3 have been considered for all the models.

2.4 Analysis Type

Both elastic buckling analysis and nonlinear static analysis were performed to estimate the critical buckling load, flexural capacity, and torsional capacity of the multi-sided tube sections. First, an eigenvalue analysis was performed using the linear perturbation buckling analysis. From the eigenvalue analysis, eigenvalues of corresponding eigenmodes were extracted. In this study, three eigenvalues for each member were obtained.

Finally, the static RIKS method (ABAQUS, 2014) was used to conduct the nonlinear buckling analysis. RIKS method is suitable for predicting buckling, post-buckling, or collapse of certain types of structures. RIKS method is based on the Arc-length method and a form of Newton-Raphson iteration method. RIKS method provides solutions for load and displacement simultaneously. From the nonlinear buckling analysis, the maximum Load Proportionality Factor (LPF) was extracted to estimate the critical buckling load. All the finite element results presented in this paper are from nonlinear static analyses.

2.5 Load Application

In this study, three different loading conditions were considered: axial compression, pure bending, and pure torsion. Axial load was applied at the top end of the member through a reference point, as shown in Fig. 2. The load was applied in the negative Z-direction to create a compressive load to the hollow column. For pure bending, a constant bending moment along the length of the member was applied about X-axis to the member. The bending moment was applied at the two reference points at each end of the multi-sided tube. For the members under pure torsion, a moment was applied at the free end about Z-axis.

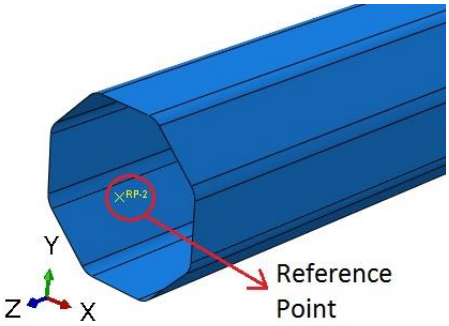

Figure 2: Reference point shown for Octagonal multi-sided tube section

2.6 Geometric Imperfection

Geometric imperfection is required to trigger buckling in the thin plates when doing FE analysis. An imperfection value of 10% of the thickness of the specimen was used for all the models. Since lowest eigenvalue refers to the load which initiates the buckling of a structure, geometric imperfection has been applied to the buckling mode obtained from the lowest eigenvalue from eigenvalue analysis (Trahair, 1993).

2.7 Residual Stress

Since welding induces residual stress into the member, residual stress needs to be considered. However, there exists minimal research on residual stress of polygonal hollow cross-sections. Fang et al. (2018) have studied residual stresses in octagonal hollow sections for different fabrication routes. In this study, residual stress pattern and values recommended by Fang et al. (2018) for octagonal hollow sections have been used. Residual stress has been incorporated in the finite element analysis as initial stress.

3. Validation of Finite Element Model

The finite element (FE) model is validated against the experiment conducted by Godat et al. (2011). Six stub columns of three different cross-sections (i.e., Octagonal, Dodecagonal, and Hexadecagonal) were tested under concentric compression. For each cross-sectional profile, two different plate width-thickness ratios were considered. Columns were simply supported with 780 mm length. To simulate the experimental results, all the geometric and mechanical properties of specimens in FEM were kept same as in the experiment. To apply the compressive load, a top plate was modeled with 10-node tetrahedral element C3D10 (ABAQUS, 2014). Both linear and nonlinear buckling analyses have been performed to estimate the critical buckling load. Imperfection values that were measured in the experimental results have been introduced in the first mode of buckling. Table 1 shows number of faces (n), plate thickness (t), flat width of plate (w), tensile yield stress (F_y), modulus of elasticity (E), yield strain (ε_y), ultimate strain (ε_u), critical buckling loads from finite element models (P_{FEM}) and experiment ($P_{Experiment}$) for the validated models. It is observed from Table 1 that the developed FE model provides excellent predictions of the local buckling capacities of multi-sided sections. As presented in Table 1, maximum difference between tests and FE analyses is about 7%.

Table 1: Geometric and Mechanical Properties of Validated Specimen

Specimen	n	t (mm)	w (mm)	F_y (Mpa)	E (GPa)	ε_y X 10^-3	ε_u (%)	P_{FEM} (KN)	$P_{Experiment}$ (KN)	% Difference
OCT-1-A	8	1.897	95	279	200	1.4	26	313.1	327	4.24
OCT-4-A	8	1.367	75	265	199	1.3	27	186.6	198	5.75
DODE-1-A	12	1.367	76	273	206	1.3	24	301.5	325	7.22
DODE-2-A	12	1.897	75	305	218	1.4	25	482.1	515	6.38
HEXA-1-A	16	1.519	52	277	199	1.4	26	319.4	317	0.75
HEXA-4-A	16	1.897	60	302	200	1.5	26	495.6	508	2.45

4. Multi-sided Tube under Different Loading Conditions

The validated finite element (FE) model has been used to conduct more analyses to observe the local buckling behavior of multi-sided tube under different loading conditions (i.e., axial compression, pure bending, and torsion) for various width-thickness ratios (b/t).

For all the FE models, element width (b), wall thickness (t), and inside bend radius (r_b) have been chosen according to AASHTO (AASHTO, 2015). AASHTO provides equation to determine the element width (b) of multi-sided tubular sections. Furthermore, according to AASHTO, multi-sided tube sections should have a minimum internal bend radius (r_b) of five times tube wall thickness or 25.4 mm, whichever is larger. Element width of multi-sided tubular sections can be found using Eq. 3:

$$b = tan\left(\frac{180}{n}\right)[D' - 2t - minimum(2r_b, 8t)] \quad (3)$$

where D' is the outside distance from the flat side to the flat side of multi-sided tubes, n is the number of sides of multi-sided tubes and $(\frac{180}{n})$ is in degrees. Fig. 3 shows the cross-section of the Octagonal section and the geometric property definition used in this study. In Fig. 3, w and D indicate the flat width and mid-surface distance from flat side to flat side of multi-sided tubes respectively.

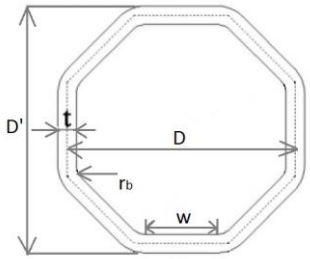

Figure 3: Cross-section of Octagonal tube section

Moreover, AASHTO has provided compact limit (λ_p), non-compact limit (λ_r), and maximum width-thickness ratio limit (λ_{max}) for the multi-sided tubes having eight (08), twelve (12) and Sixteen (16) sides. Table 2 shows the limits provided by AASHTO.

Table 2: Width-Thickness ratios for Multi-sided Tubular Sections according to AASHTO

Shape	Ratio	λ_p	λ_r	λ_{max}
Octagonal (8 sided)	b/t	$1.12\sqrt{E/Fy}$	$1.53\sqrt{E/Fy}$	$2.14\sqrt{E/Fy}$
Dodecagonal (12 Sided)	b/t	$1.12\sqrt{E/Fy}$	$1.41\sqrt{E/Fy}$	$2.14\sqrt{E/Fy}$
Hexadecagonal (16 Sided)	b/t	$1.12\sqrt{E/Fy}$	$1.26\sqrt{E/Fy}$	$2.14\sqrt{E/Fy}$

For all the FE models, element width (b) was kept the same for each polygonal section, and wall thickness (t) was varied. Moreover, b/t ratios were chosen in such a way that compact, non-compact, and slender sections could be obtained according to AASHTO. Table 3 shows the geometric properties of FE models.

Table 3: Geometric Properties of Finite Element Models

Specimen	n	b (mm)	r_b (mm)
Octagonal	8	100	Five times tube wall thickness or 25.4 mm, whichever is larger
Dodecagonal	12	95	
Hexadecagonal	16	140	

Length sensitivity analysis was conducted to get suitable lengths for each polygonal cross-section under different loading conditions. Table 4 shows the length (L) for each polygonal section under various loading conditions.

Table 4: Length of FE models for different Loading Conditions

Loading Conditions	L (mm)		
	Octagonal	Dodecagonal	Hexadecagonal
Axial Compression	1000	1200	2000
Pure Bending	2000	2500	4000
Pure Torsion	2000	2500	4000

4.1 Multi-sided Tube subjected to Axial Compression

Sixteen (16) models of each cross-section, a total of forty-eight (48) models have been analyzed under axial compression. Fig. 4 shows typical deformed shape of Octagonal, Dodecagonal, and Hexadecagonal tube sections under axial compression. Furthermore, Fig. 5 shows the critical buckling load obtained from FE models (P_{FEM}) along with the width-thickness ratio (b/t) for each polygonal section. As expected, with an increase in slenderness ratio, local buckling capacities of multi-sided tube sections decrease.

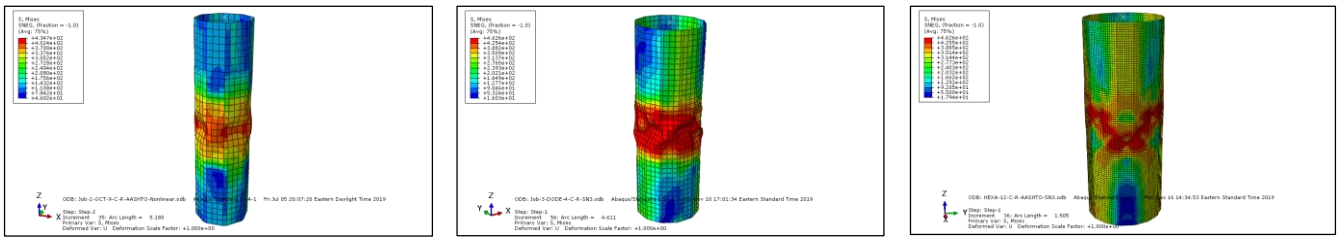

(a) Deformed shape of Octagonal section (b) Deformed shape of Dodecagonal section (c) Deformed shape of Dodecagonal section

Figure 4: Deformed shapes of multi-sided tube sections under axial compression

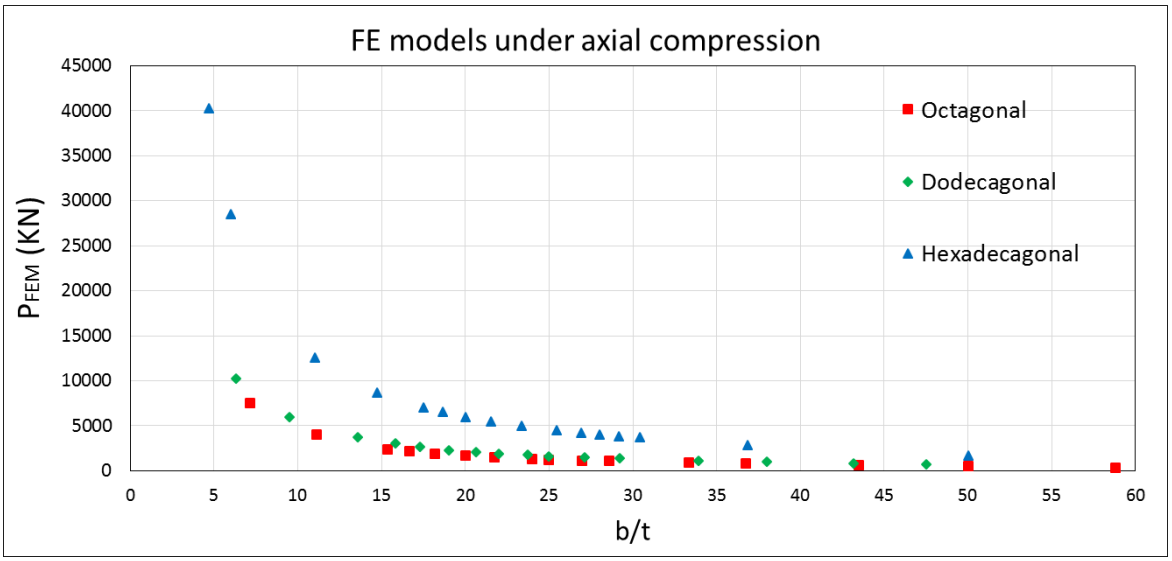

Figure 5: Critical buckling load for multi-sided tube sections under compression

4.2 Multi-sided Tube subjected to Pure Bending

Twenty-six (26) models of each cross-sectional profile, a total of seventy-eight (78) models, were subjected to uniform bending along the lengths. These models include compact, non-compact, and slender sections according to AASHTO. The local buckling deformed shape of each cross-section has been extracted from FE models. Fig. 6 shows deformed shapes of Octagonal, Dodecagonal, and Hexadecagonal sections. Furthermore, Fig. 7 shows the bending moments (M_{FEM}) obtained from nonlinear FE analyses. As shown in Fig. 7, for all three multi-sided tube shapes, bending moment capacity decreases with an increase in width-thickness ratio (b/t).

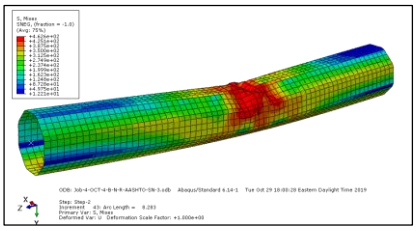

(a) Deformed shape of Octagonal section

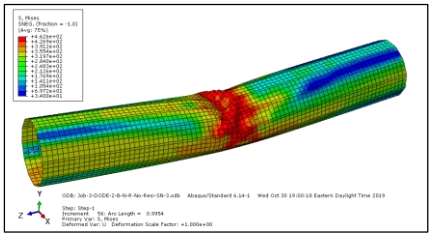

(b) Deformed shape of Dodecagonal section

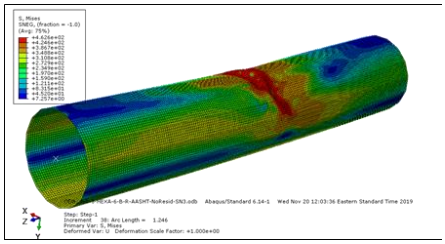

(c) Deformed shape of Hexadecagonal section

Figure 6: Deformed shapes of multi-sided tube sections under constant moment

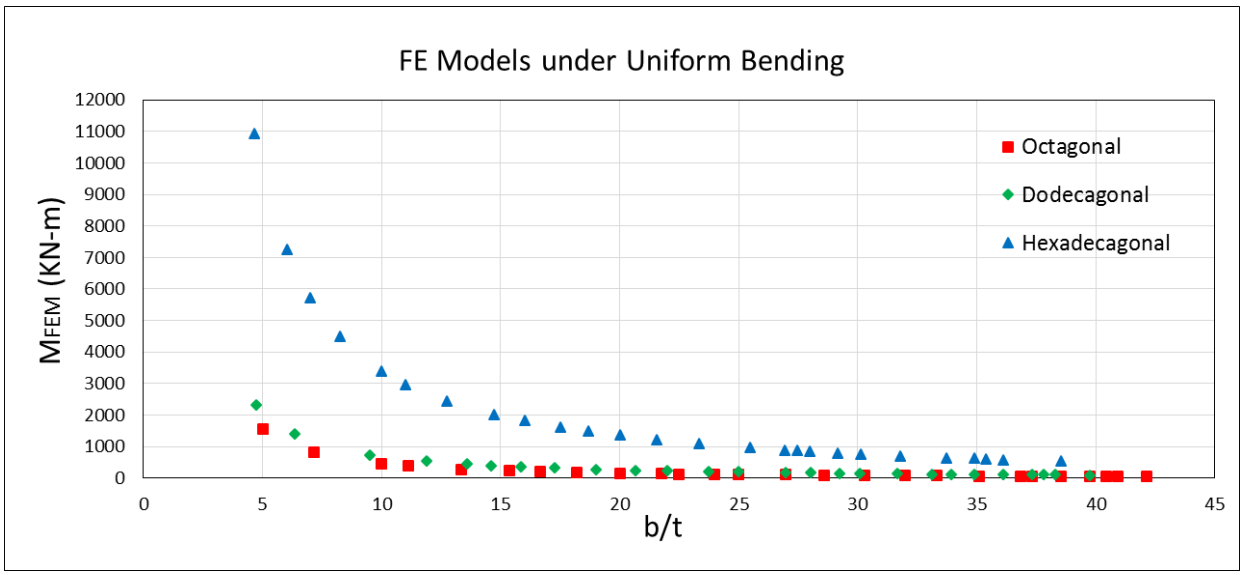

Figure 7: Critical bending capacity for multi-sided tube sections under constant moment

4.3 Multi-sided Tube subjected to Pure Torsion

Eleven (11) models of each cross-sectional profile, a total of thirty-three (33) models, were subjected to uniform Torsion. These models include both compact and non-compact sections. Following Fig. 8 shows the deformed shapes of the Octagonal, Dodecagonal and Hexadecagonal sections. Comparisons between the torsional moments obtained from FE analyses (T_{FEM}) and codes (T_{Code}) are presented in the following section.

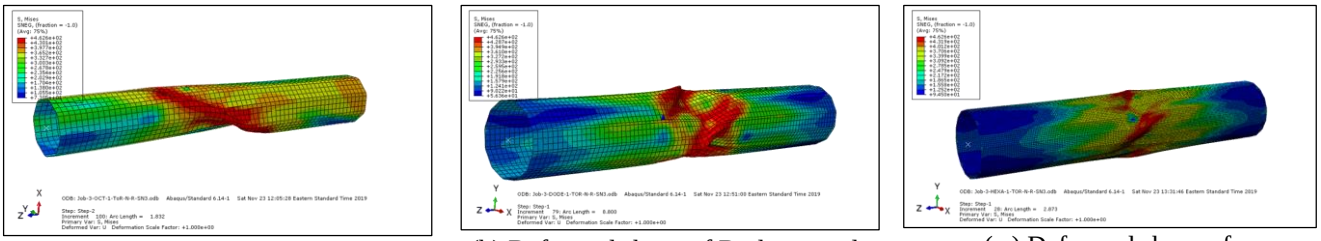

(a) Deformed shape of Octagonal section

(b) Deformed shape of Dodecagonal section

(c) Deformed shape of Hexadecagonal section

Figure 8: Deformed shapes of multi-sided tube sections under uniform torsion

5. Comparison with Codes

In this sections, results from FE models when subjected to axial compression, pure bending, and torsion were compared with different design codes.

5.1 Multi-sided Tubes under Axial Compression

Eurocode 3 (EN 1-1, 2005, EN 1-3, 2006, EN 1-5, 2006) has design equations for plate elements. A multi-sided steel tubular section has been considered as a collection of individual longitudinal plate strips to find the resistance using Eurocode 3. The design equation of EC is based on the effective area concept. According to Eurocode 3, following Eqs. (4) to (6) can be used to find the critical compressive stress (F_{cr}).

$$Aeff = \rho \times Ag \tag{4}$$

$$\rho = \begin{cases} 1, \ R \ \leq 0.5 + \sqrt{(0.085 - 0.055\psi)} \\ \frac{R - 0.055(3+\psi)}{R\hat{}2} \leq 1, \ R > 0.5 + \sqrt{(0.085 - 0.055\psi)} \end{cases} \quad (5)$$

$$F_{cr} = \rho \times F_y \quad (6)$$

where A_{eff} is an effective area, A_g is gross area, ψ is stress ratio, and plate width-thickness parameter (R) has the same definition as before.

According to AASHTO, nominal compressive strength (P_{nc}) of the multi-sided tubular column shall be calculated using Eq. 7 to Eq. 11 (AASHTO, 2015).

$$P_{nc} = A_g F_{cr} \quad (7)$$

when $\frac{KL}{r} \leq 4.71\sqrt{\frac{E}{QFy}}$; where K and r are effective length factor and radius of gyration, respectively.

$$F_{cr} = Q(0.658)^{(\frac{QFy}{Fe})} F_y \quad (8)$$

when $\frac{KL}{r} > 4.71\sqrt{\frac{E}{QFy}}$

$$F_{cr} = 0.877F_e \quad (9)$$

$$F_e = \frac{\pi^2 E}{(KL/r)^2} \quad (10)$$

If $\lambda \leq \lambda_r$, $Q=1$

If $\lambda > \lambda_r$, $Q=A_{EFF}/A_g$, where A_{EFF} is calculated from the sum of parts using effective widths (b_e)

$$b_e = 1.92t\sqrt{\frac{E}{f}}\left[1 - \frac{0.34}{\frac{b}{t}}\sqrt{\frac{E}{f}}\right] \leq b \quad (11)$$

where $f = F_{cr}$ with $Q=1$.

ASCE relies on the effective stress concept supported by the total cross-section. Its equations depend on the number of faces (ASCE/SEI-48-11, 2011). In Table 5, ϕ=6.9 and Ω= 2.62; F_y and F_{cr} are in MPa.

Table 5: ASCE Design Equations for Local Buckling Capacity of Multi-sided Tubular Column

n	Bend Angle (Degree)	b/t Limit	F_{cr} (Mpa)
4,6 or 8	≥45	$b/t \le 260\Omega/\sqrt{Fy}$	$F_{cr} = F_y$
		$260\Omega/\sqrt{Fy} < b/t \le 351\Omega/\sqrt{Fy}$	$F_{cr} = 1.42F_y(1 - 0.00114\frac{1}{\Omega}\sqrt{F_y}\frac{b}{t})$
		$b/t > 351\Omega/\sqrt{Fy}$	$F_{cr} = 104980\phi/\left(\frac{b}{t}\right)^2$
12	30	$b/t \le 240\Omega/\sqrt{Fy}$	$F_{cr} = 1.45F_y(1 - 0.00129\frac{1}{\Omega}\sqrt{F_y}\frac{b}{t})$
		$240\Omega/\sqrt{Fy} < b/t \le 374\Omega/\sqrt{Fy}$	$F_{cr} = F_y$
		$b/t > 374\Omega/\sqrt{Fy}$	$F_{cr} = 104980\phi/\left(\frac{b}{t}\right)^2$
16	22.5	$b/t \le 215\Omega/\sqrt{Fy}$	$F_{cr} = F_y$
		$215\Omega/\sqrt{Fy} < b/t \le 412\Omega/\sqrt{Fy}$	$F_{cr} = 1.42F_y(1 - 0.00137\frac{1}{\Omega}\sqrt{F_y}\frac{b}{t})$
		$b/t > 412\Omega/\sqrt{Fy}$	$F_{cr} = 104980\phi/\left(\frac{b}{t}\right)^2$

FE analysis results were compared with the compressive resistance provided by different codes, as shown in Fig. 9. Moreover, the ratio of compressive stress obtained from the FE model (F_{FEM}) and yield stress (F_y) is plotted in the same graph along with the non-compact limit (λ_r) provided by AASHTO for different multi-sided tubes (Fig. 10).

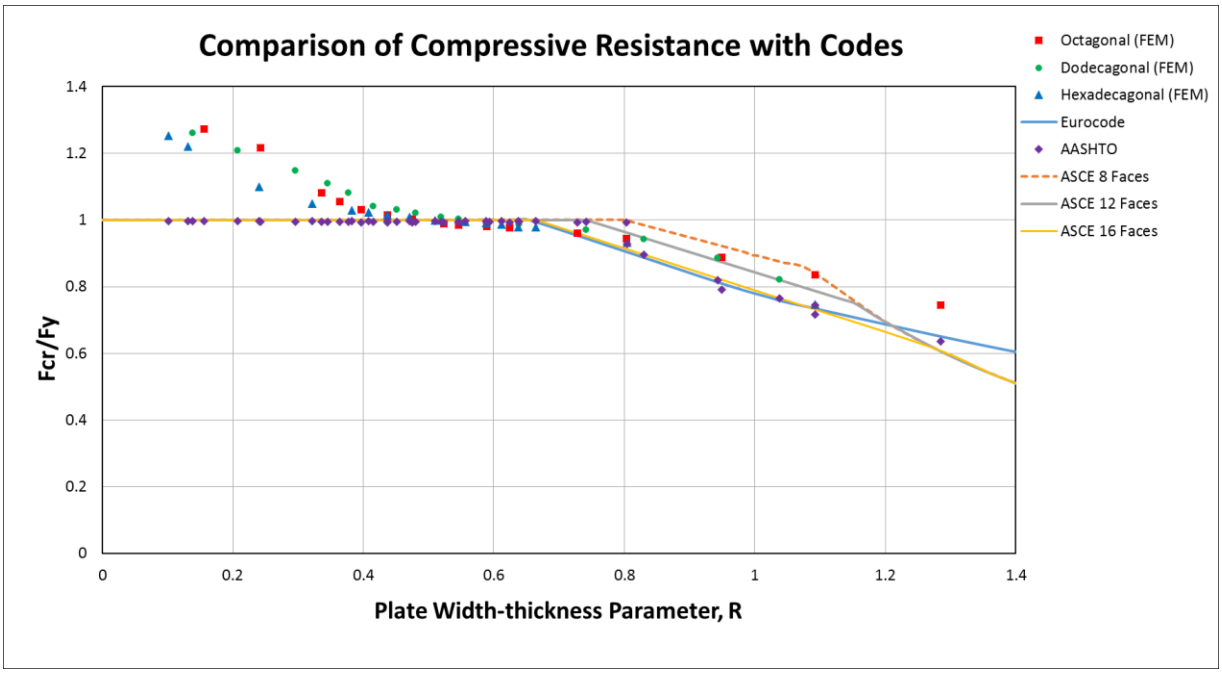

Figure 9: Comparison of compressive resistance from FE analysis with different codes

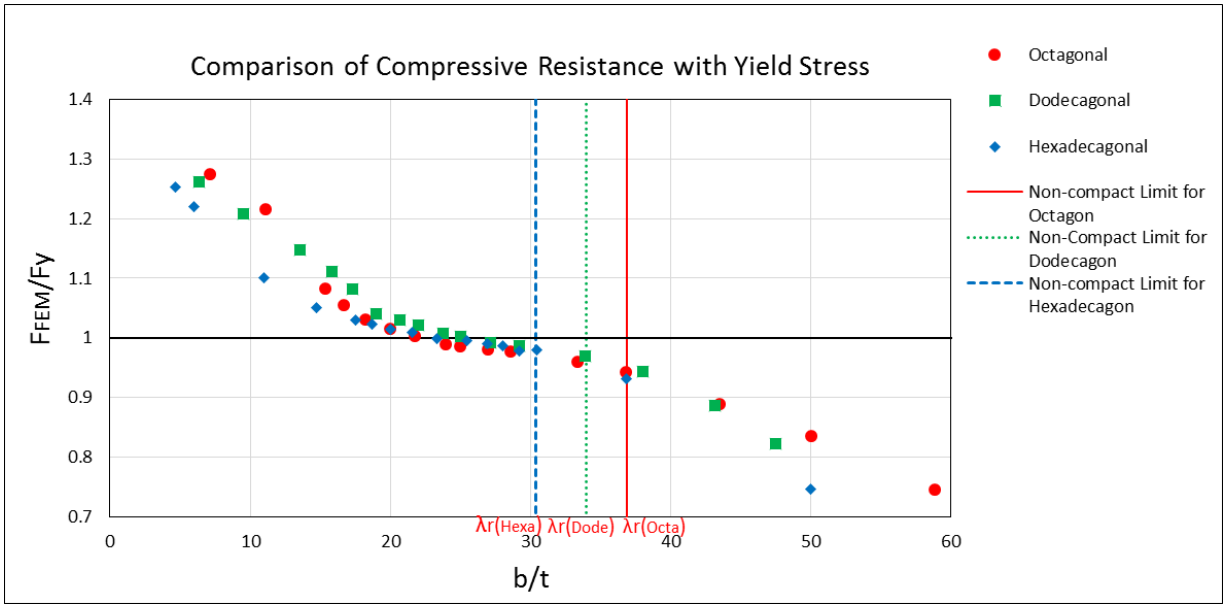

Figure 10: Comparison of compressive resistance from FE analysis with yield stress

5.2 Multi-sided Tubes under Pure Bending

For each model subjected to pure bending, plastic moment capacity (M_p) and elastic moment capacity (M_y) have been calculated. Fig. 11 shows the comparison of the bending capacity of the FE model (M_{FEM}) with the plastic moment (M_p). Compact Limit (λ_p) of AASHTO has been shown in Fig. 11.

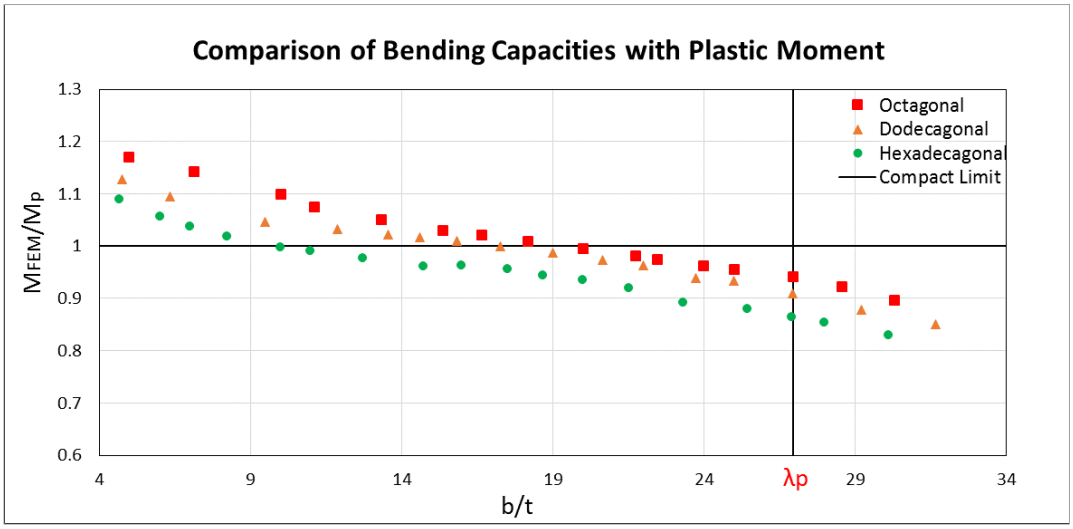

Figure11: Comparison of bending capacity from FE analysis with plastic moment capacity

Fig. 12, 13 and 14 present the comparisons of the bending capacities of the non-compact and slender sections with the elastic moments for Octagonal, Dodecagonal, and Hexadecagonal sections, respectively. In the following figures, the compact and non-compact limits of AASHTO are indicated.

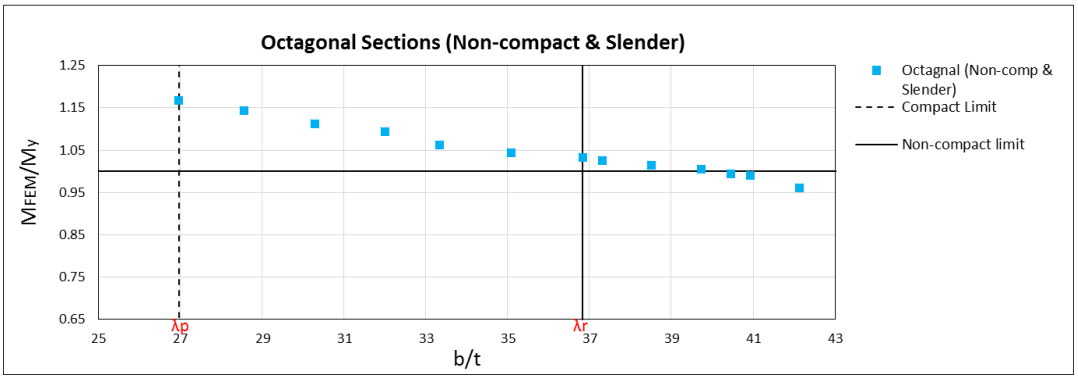

Figure12: Comparison of Octagonal non-compact and slender section with yield moment

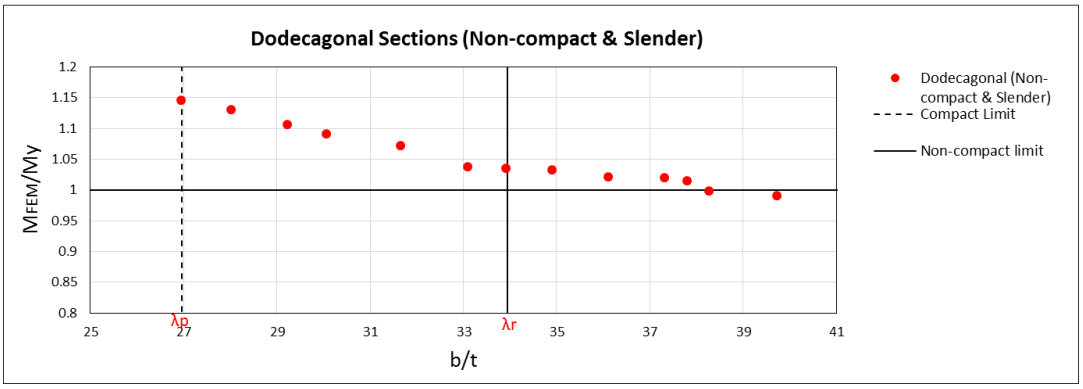

Figure13: Comparison of Dodecagonal non-compact and slender section with yield moment

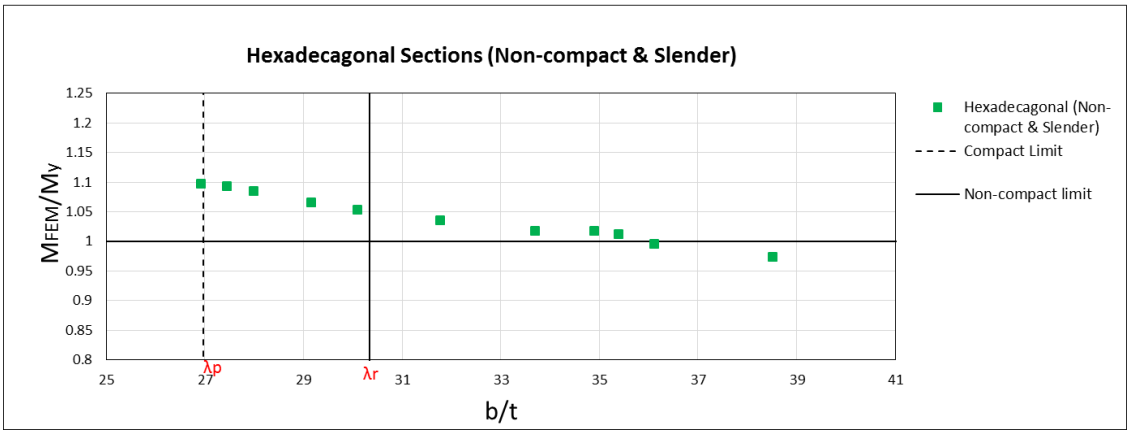

Figure 14: Comparison of Hexadecagonal non-compact and slender section with yield moment

5.3 Multi-sided Tubes under Pure Torsion

According to AASHTO, nominal torsional strength (T_n) shall be computed using the following Eq. 12:

$$T_n = C_t\, F_{nt} \tag{12}$$

where T_n is nominal torsion strength, C_t is the torsional constant, and F_{nt} is the nominal torsional stress capacity. Torsional Constant (C_t) shall be computed by using Table 6. The nominal torsional stress capacity (F_{nt}) for multi-sided tubular shapes shall be:

$$F_{nt} = 0.6\, F_y \tag{13}$$

Table 6: Torsional Constant for Stress Computation

	Octagonal	Dodecagonal	Hexadecagonal
Torsional Constant (C_t) for stress computation	$\frac{6.63R'^2t}{k_t}$	$\frac{6.43R'^2t}{k_t}$	$\frac{6.37R'^2t}{k_t}$

In Table 6, k_t indicates stress concentration factor, and it should be determined using the following Eq.14:

$$k_t = \frac{t}{R'}\left[\frac{\frac{R'}{n't}-\frac{1}{2}\left(1+\frac{n'+1}{n'}\right)}{ln\left(\frac{n'+1}{n'}\right)}\right] + \frac{n't}{R'} \geq 1 \tag{14}$$

where R' is radius measured to the mid-thickness of the wall and n' is the ratio of the inside-corner radius to wall thickness.

According to ASCE, nominal torsional strength (T_n) shall be computed using the following Eq. 15:

$$T_n \leq F_v \frac{J}{c} \tag{15}$$

$$F_v = 0.58\, F_y \tag{16}$$

where F_v is shear stress permitted, c is the distance from the neutral axis to extreme fiber, and J is the torsional constant of cross-section. The maximum value of c/J is defined in ASCE and is shown in Table 7.

Table 7: Maximum value of c/J according to ASCE

	Octagonal	Dodecagonal	Hexadecagonal
Max c/J	$\frac{0.603(D+t)}{D^3 \times t}$	$\frac{0.622(D+t)}{D^3 \times t}$	$\frac{0.628(D+t)}{D^3 \times t}$

For all the sections, torsional capacities have been calculated according to AASHTO and ASCE. Fig. 15 shows the ratio of Torsional moments obtained from FE models and two codes (i.e. AASHTO and ASCE) along with width-thickness ratios for Octagonal, Dodecagonal and Hexadecagonal sections.

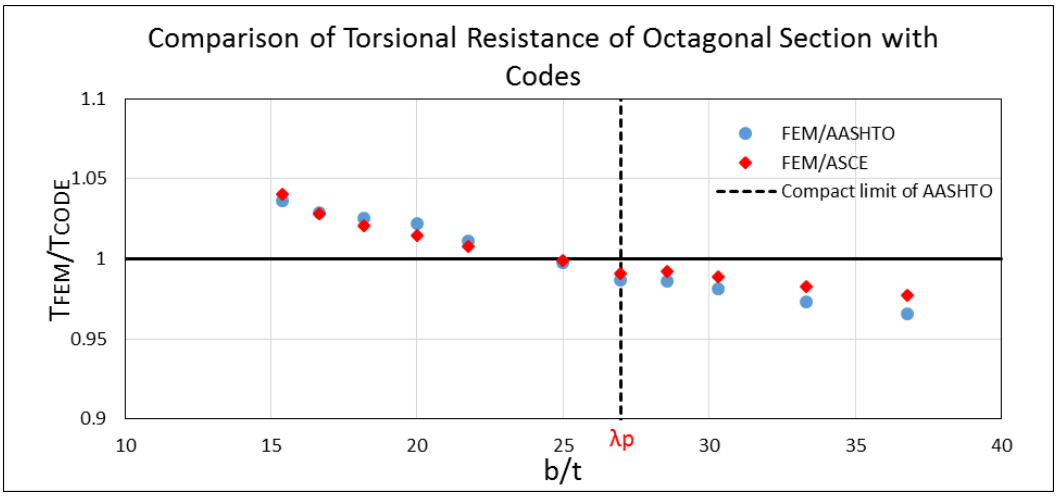

(a) Torsional resistance of Octagonal section

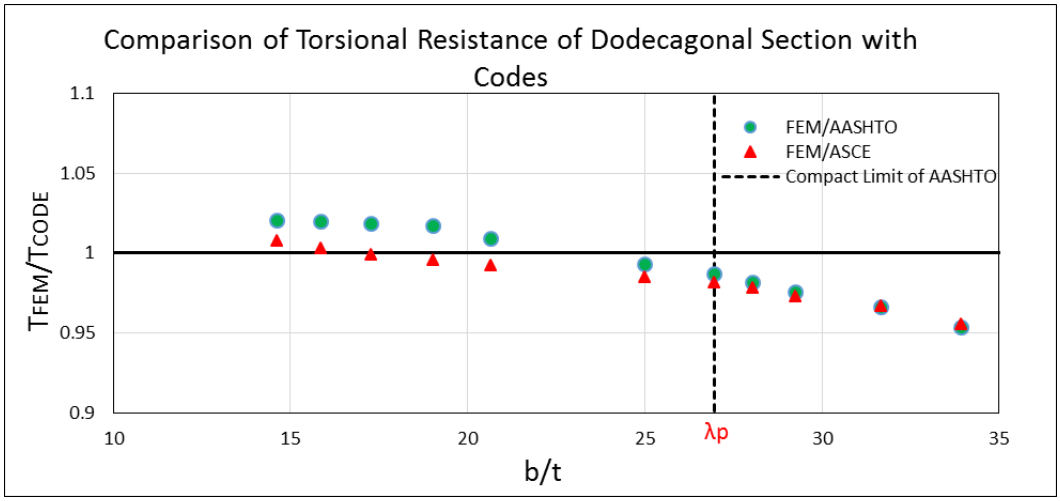

(b) Torsional resistance of Dodecagonal section

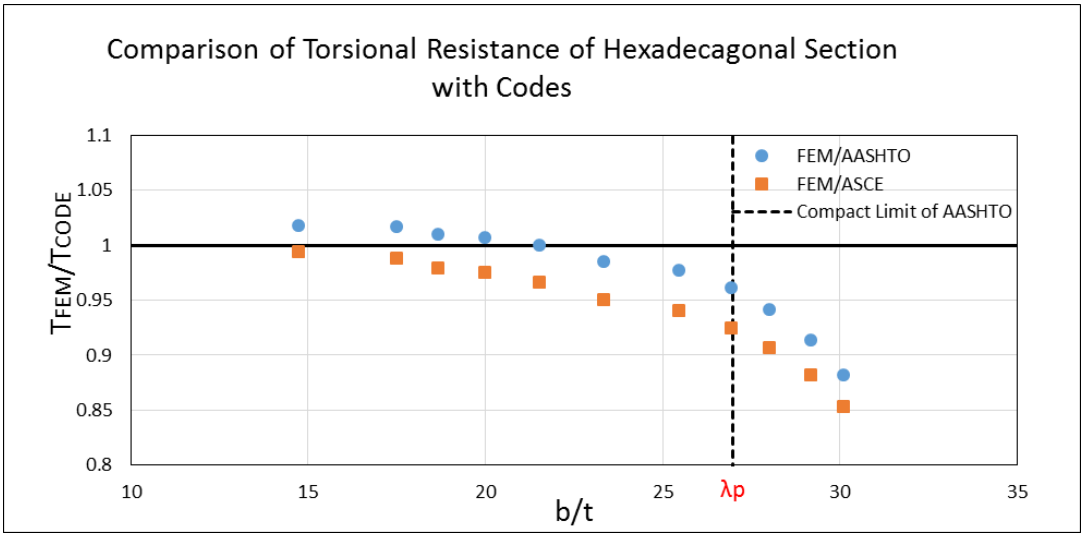

(c) Torsional resistance of Hexadecagonal section

Figure 15: Comparison of torsional resistance of multi-sided sections with codes

6. Discussion on Results

Comparison between results from FE models under axial compression and three codes (Fig. 9) show that up to Plate width-thickness parameter (*R*) value of 0.66, FE analyses provide capacities either close to the three codes or higher than the codes, indicating that codes' equations for compressive resistance are conservative in this range. Beyond the R-value of 0.66, ASCE provides three different curves for 8, 12, and 16-sided sections. Fig. 9 also shows that both AASHTO and Eurocode provide good predictions for the compressive resistance for multi-sided tube sections. In addition, for octagonal section, ASCE predictions are higher than that obtained from FE analyses.

Moreover, Fig. 10 shows the comparison between the FE model results under axial compression and yield stress (F_y). Though AASHTO has provided three different non-compact limits (λ_r) for different cross-sections, all sections having a width-thickness ratio (b/t) within the non-compact limit of Hexadecagonal section could reach capacities close to yield stress (F_y). This means using the non-compact limit of the Hexadecagonal section for all three sections under axial compression is safer.

Fig. 11 shows comparison of the bending capacities of multi-sided tube sections with the plastic moment capacities (M_p). AASHTO has the same compact limit (λ_p) for Octagonal, Dodecagonal, and Hexadecagonal multi-sided tube sections. However, results show that several compact sections (according to AASHTO) are not able to reach plastic moment capacity. The number of compact sections not reaching plastic moment is increasing with the increasing number of sides. It indicates a revision may be required for the compact limit (λ_p) suggested by AASHTO for sections subjected to pure bending.

Fig. 12, 13, and 14 show the comparisons of the bending capacities of non-compact and slender sections with elastic moment capacities (M_y) for Octagonal, Dodecagonal, and Hexadecagonal section, respectively. AASHTO has provided three different non-compact limits (λ_r) for the Octagonal, Dodecagonal, and Hexadecagonal section. From these figures, it is observed that all the non-compact sections, along with some slender sections, could reach elastic moment capacities. It implies that AASHTO provided non-compact limits are quite relaxed for the sections subjected to pure bending.

Fig. 15 shows the comparison between FE models subjected to torsion and codes (i.e., AASHTO and ASCE). FE models of Octagonal compact sections mostly have higher capacities than the AASHTO, and ASCE suggested torsional capacities. However, Octagonal non-compact FE models are not capable of reaching the capacities indicated by the two codes. For Dodecagonal compact sections, most of the sections could reach capacities higher than AASHTO provided capacities. The ratios of capacity from the FE models and ASCE are close to 1.0 for most of the compact Dodecagonal sections. However, the FE models of Dodecagonal compact sections near the non-compact limit and for all the non-compact sections have lower capacities than AASTO and ASCE, indicating codes are overestimating to some extent. It is also observed from Fig. 15 that ASCE provides higher capacities for Hexadecagonal sections. Except for very few of the Hexadecagonal compact sections, AASHTO also provides higher torsional capacities than the FE analysis results.

7. Conclusions

This paper presented a finite element (FE) analysis based study of local buckling of multi-sided steel tubular sections. A nonlinear finite element model was developed to analyze a series of multi-sided steel tubular sections under axial compression, pure bending and pure torsion. Three different geometry, namely, eight, twelve and sixteen-sided polygonal sections were considered. Both linear buckling and nonlinear static analyses were conducted using ABAQUS. Comparison between FE models under axial compression results and three codes (i.e., AASHTO, Eurocode and ASCE) showed that, up to Plate width-thickness parameter (R) value of 0.66, FE model provided capacity either close to the three codes or higher than codes, indicating code equations are conservative in this range. AASHTO has provided compact, non-compact and maximum width-thickness limits for Octagonal (8-sided), Dodecagonal (12-sided), and Hexadecagonal (16-sided) tube sections. While the maximum width-thickness limit for compact sections is the same regardless of the number of sides, the non-compact limit is different for three sections. The comparison between FE models under axial compression and yield stress indicate that using the non-compact limit of Hexadecagonal section for all the three sections under axial compression is safer. Moreover, the comparison between the capacities of compact FE models under pure bending and plastic moment shows that the compact limit of AASHTO may need to be revised to a lower limit. For non-compact sections under bending, the slenderness limits provided by AASHTO are conservative and can be revised to a higher value. Also, similar to compact limit, same non-compact limit can be used for all three shapes. For the models subjected to torsion, except for some of the compact sections, both AASHTO and ASCE provide higher torsional strength than FE analysis results for Octagonal, Dodecagonal, and Hexadecagonal multi-sided tube sections.

Acknowledgments

Funding for this research project is provided by the Faculty of Engineering and Computer Science, Concordia University, Montreal, Canada and the Natural Sciences and Engineering Research Council of Canada. The authors gratefully acknowledge Dr. Gilbert Y. Grondin for his valuable suggestions in this research.

References

ABAQUS. (2014). ABAQUS standard user's manual, 6.14. Dassault Systèmes.

American Association of State Highway and Transportation Officials (AASHTO). (2015). LRFD Specifications for Structural Supports for Highway Signs, Luminaires, and Traffic Signals, Washington, DC.

American Society of Civil Engineers (ASCE). (2011). Design of Steel Transmission Pole Structures, ASCE/SEI 48-11, Reston, Virginia.

Aoki, T., Migita, Y., and Fukumoto, Y. (1991). "Local buckling strength of closed polygon folded section columns." *Journal of Constructional Steel Research*, 20 (4) 259–270.

Bräutigam, K., Knoedel, P., and Ummenhofer, T. (2017). "Plastic behaviour of polygonal hollow sections in bending." *Steel Construction*, 10 (3) 222-226.

Eurocode 3. (2005). EN 1993-1-1 Eurocode 3: Design of steel structures - Part 1–1: general rules and rules for buildings. European Committee for Standardization (CEN), Brussels, Belgium.

Eurocode 3. (2006). EN 1993-1-3 Eurocode 3: Design of steel structures - Part 1–3: General rules- Supplementary rules for cold-formed members and sheeting. European Committee for Standardization (CEN), Brussels, Belgium.

Eurocode 3. (2006). EN 1993-1-5 Eurocode 3: Design of steel structures - Part 1–5: General rules - Plated structural elements. European Committee for Standardization (CEN), Brussels, Belgium.

Fang, H., Chan, T., and Young, B. (2018). "Material properties and residual stresses of octagonal high strength steel hollow sections." *Journal of Constructional Steel Research*, 148, 479–490.

Godat, A., Legeron, F., and Bazonga, D. (2012). "Stability investigation of local buckling behavior of tubular polygon columns under concentric compression". *Thin-Walled Structures*, 53, 131-140.

Gonçalves, R., and Camotim, D. (2013). "Elastic buckling of uniformly compressed thin-walled regular polygonal tubes." *Thin-Walled Structures*, 71, 35-45.

Teng, J.G., Smith, S.T., and Ngok, L.Y. (1999). “Local buckling of thin-walled tubular polygon columns subjected to axial compression or bending.” *Proceedings of the Second International Conference on Advances in Steel Structures*, Elsevier Steel Structures Division, Hong Kong, China, 1, 109–115.

Timoshenko, S.P., and Gere J. M. (1961). “Theory of elastic stability.” 2nd ed., McGraw Hill, New York, NY, USA.

Trahair, N. S. (1993). “Flexural-Torsional buckling of structures.” *CRC Press*, Boca Raton, FL.

Wittrick, W. H., and Curzon, P. L. V. (1968). “Local buckling of long polygonal tubes in combined bending and torsion.” *International Journal of Mechanical Sciences*, 10, 849-857.